THE JOURNAL OF PHYSICAL CHEMISTRY B

ARTICLE

pubs.acs.org/JPCB

Effects of Anions on Nanostructuring of Cationic Amphiphilic Peptides

Meiwen Cao,[†] Yuming Wang,[†] Xin Ge,[†] Changhai Cao,[†] Jing Wang,[†] Hai Xu,[*,†] Daohong Xia,[†] Xiubo Zhao,[‡] and Jian R. Lu[*,‡]

[†]Centre for Bioengineering and Biotechnology, China University of Petroleum (East China), 66 Changjiang West Road, Qingdao Economic Development Zone, Qingdao 266555, People's Republic of China

[‡]Biological Physics Laboratory, School of Physics and Astronomy, University of Manchester, Schuster Building, Manchester M13 9PL, United Kingdom

Supporting Information

ABSTRACT: The effects of addition of a series of stoichiometric salts on the nanostructuring of cationic amphiphilic peptides have been investigated through the combination of atomic force microscopy (AFM), circular dichroism (CD), and turbidity measurements. The results revealed that anions had more pronounced effects than cations in tuning the nanostructures formed from these peptides. Addition of ClO_3^-, NO_3^-, and Br^- could stabilize the primary nanostructures (nanostacks, nanospheres, or short nanorods) formed by A_9K and I_3K and effectively inhibit their growth into longer nanostructures (nanorods or nanotubes). In contrast, the anions of Cl^-, SO_4^{2-}, HPO_4^{2-}, PO_4^{3-}, and $C_6H_5O_7^{3-}$ (citrate) favored the axial growth of these peptides to form long intersecting nanofibrils and led to an increase in diameter and surface roughness, as well, clearly enhancing their propensity for nanostructuring. The efficiency of different anions in promoting the growth of peptide nanoaggregates into larger ones could be ordered as $ClO_3^- < NO_3^- \leq Br^- < Cl^- < SO_4^{2-} < HPO_4^{2-} < PO_4^{3-} < C_6H_5O_7^{3-}$, broadly consistent with the Hofmeister anion sequence. These observations were well rationalized by considering different aspects of direct interactions of the anions with the peptide molecules.

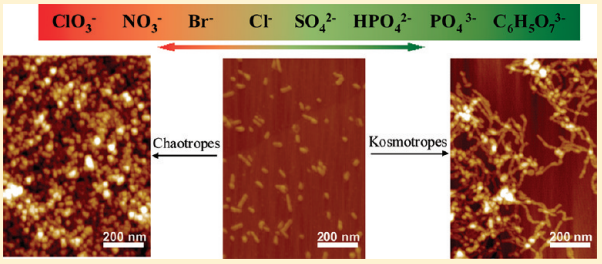

INTRODUCTION

Molecular self-assembly is the spontaneous organization of molecules into ordered structures by weak noncovalent interactions including hydrogen bonding, van der Waals force, electrostatic interaction, hydrophobic interaction, and aromatic $\pi-\pi$ stacking. Such a process is ubiquitous in nature to achieve a rich variety of ingenious structural assemblies to function as molecular and cellular machines.[1] Molecular self-assembly has now developed into a promising "bottom-up" approach for fabricating biomimetic and bioinspired nanostructures[2,3] as well as macroscopic functional materials.[4]

Amphiphilic peptides, also known as surfactant-like peptides,[5−7] are a novel class of self-assembling molecules that have attracted considerable interests in the past decade.[8−10] These peptides bear a distinct similarity to natural lipids but use hydrophobic amino acids as building blocks to make up the hydrophobic moiety and polar and charged amino acids to make up the hydrophilic moiety. These peptide amphiphiles can readily undergo self-assembly to form well-defined nanostructures such as nanofibers, nanotubes, ribbons, and vesicles. These nano- and micro-organizations may further integrate into different three-dimensional networks.[5,6,8,9] Because of their well-ordered structures, inherent bioactivity, biocompatibility, and chemical and biological modifiability, peptide assemblies exhibit great potential in a wide range of technological applications including templates for fabrication of nanostructured hybrids and/or inorganic materials,[9,11−13] scaffolds for tissue engineering,[3] delivery vectors for drugs and genes,[14,15] agents for membrane protein stabilization[16,17] and antibacterial application.[18]

Fabrication with fine control of self-assembled structures is crucial toward empowering their functionalities and developing attractive applications.[19] From a fundamental chemical perspective, the starting step for tuning peptide self-assembly is typically to tailor their molecular structures. Zhang and co-workers[5] have controlled the self-assembly of surfactant-like peptides into nanotubes or nanovesicles by modifying the hydrophobic moiety of amino acids and the charge number of the hydrophilic moiety. We have further demonstrated the transitions in the self-assembled nanostructures of amphiphilic peptides A_mK_n by varying the length of hydrophobic and hydrophilic moieties and using hydrophobic amino acids of different sizes.[8] Subsequently, a variety of external chemical and physical triggers have been used to modulate peptide self-assembly. Carrick et al.[20] have found that ionic strength can influence the self-assembly, morphology, and gelation of some β-sheet tape-forming peptides. Song et al.[21] and Yan et al.[22,23] have harnessed the transitions

Received: January 15, 2011
Revised: September 5, 2011
Published: September 06, 2011

between nanotubes and vesicle-like structures of Phe−Phe dipeptides through varying concentration. Yang et al.[24] have demonstrated that both metal ions and anions can greatly change the nanostructures of self-assembling peptide EAK16(II)GGH. Others have also reported stimuli-responsive self-assembly of peptides depending on environmental conditions such as pH, temperature, ionic strength, light, and oxidation/reduction state.[25,26]

Hofmeister effects are frequently used to explain the effects of various ions on protein solubility and structural stability. The sequence that ranks the relative effectiveness of specific ions is often termed the Hofmeister series.[27] The term "chaotrope" was first coined by Hamaguchi and Geiduschek,[28] and the term "kosmotrope" was first coined by Collins and Washabaugh.[29] Chaotrope means only "weakly hydrated". In contrast, the behavior of the kosmotrope refers to the local effect of strong binding of the immediately adjacent water molecules. In most common conditions, where no specific (direct) ion binding is involved, kosmotropic ions help stabilize protein structure in aqueous solution while chaotropic ions often deteriorate protein structure.[30−32] Experimental observations suggest that the effects of chaotropic and kosmotropic ions on protein stability result from direct binding (typically at ion concentrations below 0.2 M) and water-mediated indirect interfacial interactions (at ion concentrations higher than 0.2 M) between ions and proteins.[30,33−35] These effects, often termed "salting in" and "salting out", are also found to affect enzymatic activities,[36,37] surface adsorption, and solution aggregation.[38−40]

By tuning their molecular structures of peptide amphiphiles, we have recently shown interesting structural transitions from unstable lamellar stacks (incapable of holding water hydration) formed by A_3K, long and stable nanofibers by A_6K, to nanorods by A_9K (diameters around 3 nm and lengths around 100 nm), all in aqueous solution.[8,41] Since trifluoroacetic acid (TFA) was used to cleave the peptide from the resin during our peptide synthesis, the finally purified peptide products are in the form of trifluoroacetate salts. Bucak et al.[42] and our group[8,41] have shown that A_6K in the form of trifluoroacetate salt tended to self-assemble in aqueous solution to form uniform tubular nanostructures and the diameters of these tubes depended on peptide concentration and end-capping form. In this work, we assess the effects of different ions on the peptide self-assembly by adding a stoichiometric amount of salt into peptide solution. Because CF_3COO^- existed as the counterion of the peptides and worked effectively as a background ion, we assume it did not affect the main trends of the specific ion efficiency order in promoting peptide aggregation. Our results indicate that the order of efficiency of different anions in promoting peptide aggregation coincides well with the well-established Hofmeister sequence, which indicates a general strategy for the tuning of the self-assembly of cationic amphiphilic peptides through adjustment of anions.

EXPERIMENTAL SECTION

Materials. The peptides (A_6K, A_9K, I_3K, and I_4K) (A, alanine; K, lysine; I, isoleucine) were synthesized according to the method reported previously.[8] After cleavage of the peptide from resin with a mixture of TFA, triisopropylsilane, H_2O, and ethanedithiol in a ratio of 94:1:2.5:2.5, the rough product dissolved in DCM was rotary evaporated to a concentrated solution and then precipitated by adding cold ethyl ether. The solid products were collected by centrifuging the ether solution, and the cold ether washing and centrifuging were repeated until the pH of the supernatant fluid remained constant at pH 5−6. The final peptide products were lyophilized for 2 days, and their purity was checked by reversed-phase HPLC (Waters 2695 Alliance HPLC system) and MALDI-ToF-MS (Bruker Biflex III matrix) and was above 98% in each case. All of the salts used ($NaClO_3$, $NaNO_3$, NaBr, NaCl, Na_2SO_4, Na_2HPO_4, $Zn(NO_3)_2$, $ZnCl_2$, $ZnSO_4$, Na_3PO_4, and $Na_3C_6H_5O_7$ (trisodium citrate)) were purchased from Sinopharm Chemical Reagent Company (SCRC) with purity >99.0%. Pure water (18 MΩ cm^{-1}) was obtained from the Milli-Q system and used throughout the experiments. All of the experiments were carried out at ambient temperature around 20 °C if not specified.

Preparation of Peptide Solutions. Peptide stock solutions and salt stock solutions were prepared by dissolving dry samples directly in pure water. Both peptides and salts showed high water solubility, and no visible precipitates were observed during our measurements. The peptide solutions as prepared were slightly acidic with pH around 6. A minute amount of dilute NaOH solution was then used to adjust solution pH to 7. Note that no buffering was used for these solutions to avoid its interference. Peptide solution and appropriate salt solution were mixed together in any given ratios to reach the concentrations as required. It was noted that such mixing could cause pH rising, but in all cases, the pH values were all within 7−8 (Supporting Information Table S1). Prior to AFM measurements and other characterizations, peptide solutions were incubated for 1 week in order to make sure that the peptide assembly attained its equilibration.

Atomic Force Microscopy (AFM). A Multimode Nanoscope IVa AFM (Digital Instruments, Santa Barbara, CA) was used for AFM measurements under ambient conditions. The probes used were TESP silicon probes (Veeco, Santa Barbara, CA) with a nominal spring constant of 42 N/m. For sample preparation, 10−15 μL peptide solution was deposited onto a freshly cleaved mica surface. After 5−60 s, excessive liquid was removed from the mica surface, followed by drying with a gentle stream of nitrogen. After sample preparation, the surface was immediately subjected to AFM imaging. Tapping mode images were obtained with a scan speed of 1.0−1.8 Hz, a tip resonance frequency of 230−300 kHz, and drive amplitude of 20−100 mV. Topographic data were regularly recorded as 512 × 512 pixel images simultaneously in trace and retrace to check for scan artifacts. Analysis of the images was carried out using the Digital Instruments Nanoscope software (version V530r3sr3). All images are shown without any treatment except the first-order flattening to remove any tilt in the surface.

Turbidity Measurements. Turbidity measurements were carried out with a UV−vis spectrophotometer (UV-1700 Phama Spec, Shimadzu) at the ambient temperature around 20 °C. The turbidity of the peptide solutions in the presence of different salts was monitored by following UV absorbance at 350 nm from a cuvette with 1 cm path length.

Circular Dichroism (CD). CD spectra were recorded on a spectrophotometer (MOS-450/AF-CD, BioLogic) at the ambient temperature of 20 °C using a 1.0 mm quartz cell. Scans were obtained between 190 and 250 nm by taking points at 0.5 nm, with an integration time of 0.5 s. The spectra were smoothed using the noise reducing option in the software supplied by the vendor. The spectroscopic scan was repeated at least three times, and their average results are presented.

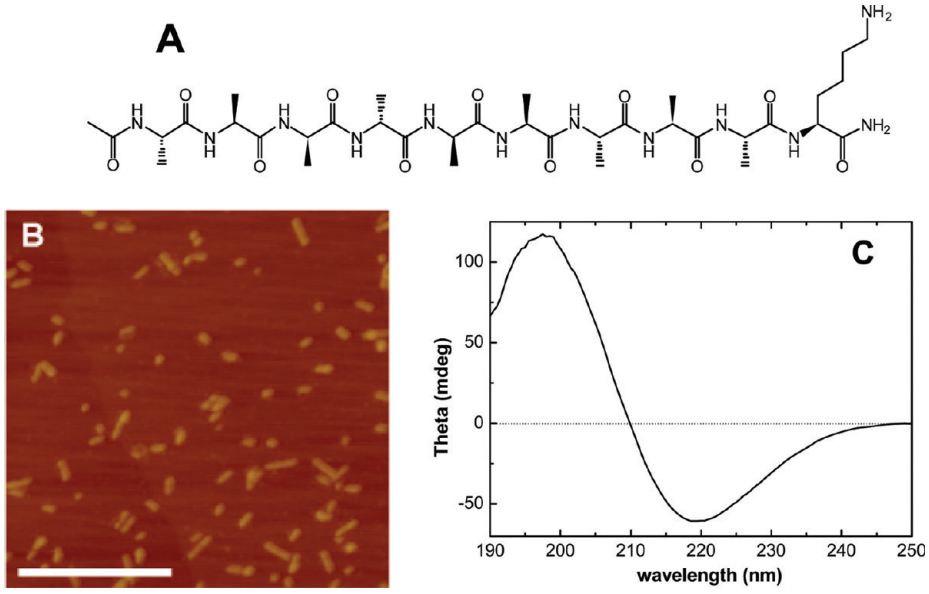

Figure 1. (A) Molecular structure of A_9K. (B) AFM height image (scale bar = 500 nm, height scale = 30 nm) of the self-assembled structures of A_9K at 1.0 mM and pH 7.0. (C) CD spectrum of the A_9K aqueous solution. The pH was adjusted by adding a minimal amount of NaOH solution.

RESULTS

Self-Assembly of A_9K. The molecular structure of A_9K is presented in Figure 1A. This molecule comprises the hydrophobic moiety consisting of nine consecutive alanine residues and the hydrophilic moiety formed by a lysine residue. Both ends of the polypeptide chain are blocked by acetyl and amide groups so that the molecule carries only one positive charge on the K residue around pH 7 (the pK_a for lysine is around 10.3). Nanostructuring is driven through self-assembly via hydrophobic affinity between the hydrophobic tails, associated with electrostatic repulsion between the head K groups and hydrogen bonding due to the intrinsic nature of the amide bonds. The size and shape of the assembled nanostructures are determined by the subtle balances between these noncovalent interactions.

As evident from Figure 1B, two types of self-assembled structures were formed from A_9K: the nearly spherical aggregates or nanostacks (as intermediates) and the short rod-like structures (nanorods). The nanostructuring occurred at 1.0 mM A_9K and pH 7.0. AFM height profiling showed that the heights of both nanostacks and nanorods remained almost constant at 3.2 ± 0.6 nm, in good agreement with our previous findings.[8,41] The CD spectrum (Figure 1C) reveals a typical β-sheet secondary structure from the self-assembled system,[43] characterized by a positive maximum at 198 nm and a negative minimum at 219 nm. The equilibration between the two types of nanostructures makes the system ideal for investigating the possible factors that affect the dynamic self-assembly process.

Effect of Sodium Salts with Different Anions on the Self-Assembly of A_9K. Figure 2 shows the topographical AFM images of the A_9K (1.0 mM) nanostructures formed in the presence of sodium salts (the Na^+ concentrations were fixed at 1.0 mM in all of the investigated cases) with different anionic counterions. The characteristic structural parameters derived from these images are summarized in Table 1, together with the ones from the control experiment (Figure 1B, without added salt) for comparison. AFM profiling was again used to estimate the heights of the aggregate species. Clearly, the self-assembled structures of A_9K depend significantly on the salt species used. As already outlined, in the absence of salt (control), the self-assembled structures had heights of 3.2 ± 0.6 nm and lengths of smaller than 100 nm. In the presence of salts, however, the nanostructures of A_9K changed significantly and the morphologies varied with respect to different salts. In the cases of $NaClO_3$, $NaNO_3$, and NaBr (Figure 2A−C), for instance, only spherical stacks were obtained, all showing slightly larger heights, which are 3.7 ± 0.5 nm for $NaClO_3$, 4.0 ± 0.6 nm for $NaNO_3$, and 3.8 ± 0.8 nm for NaBr, respectively. In the cases of NaCl, Na_2SO_4, Na_2HPO_4, Na_3PO_4, and $Na_3C_6H_5O_7$, however, relatively long fibrils occurred with lengths mostly larger than 500 nm and heights of 4.0−5.5 nm (Figure 2D−H). These latter fibrils were rather flexible and were not uniform along their lengths, resembling beaded fibrils, suggesting that the fibrils are formed by the association of spherical stacks and short nanorods, similar to the evolution of amyloid fibrils.[44] No matter what kinds of salts are present, one common feature is that the formed structures showed higher extent of lateral association.

Since the cation was fixed, the salt effects can simply be attributed to the effects of the different anions. The above results indicate that Cl^-, SO_4^{2-}, HPO_4^{2-}, PO_4^{3-}, and $C_6H_5O_7^{3-}$ favor the axial growth of the A_9K nanostructures, which could well arise from the alignment and attachment of the short nanostacks to form nanorods. Such end-to-end alignment and growth could be driven by the need to heal end defects, resulting in further energy minimization. In contrast, ClO_3^-, Br^-, and NO_3^- seemed to stabilize the spherical nanostacks and inhibit the axial growth, suggesting a different mode of ion interaction.

Increase in ionic strength by addition of salts to the solution results in the reduction of electrostatic repulsion between the charged head groups of A_9K molecules due to charge screening. This process usually disfavors the curvature of the assembled structures and leads to an increase in the diameter of the nanostructures, though the effect does not seem to alter their shape significantly. Charge screening would also reduce repulsion between neighboring nanostacks and nanorods, promoting

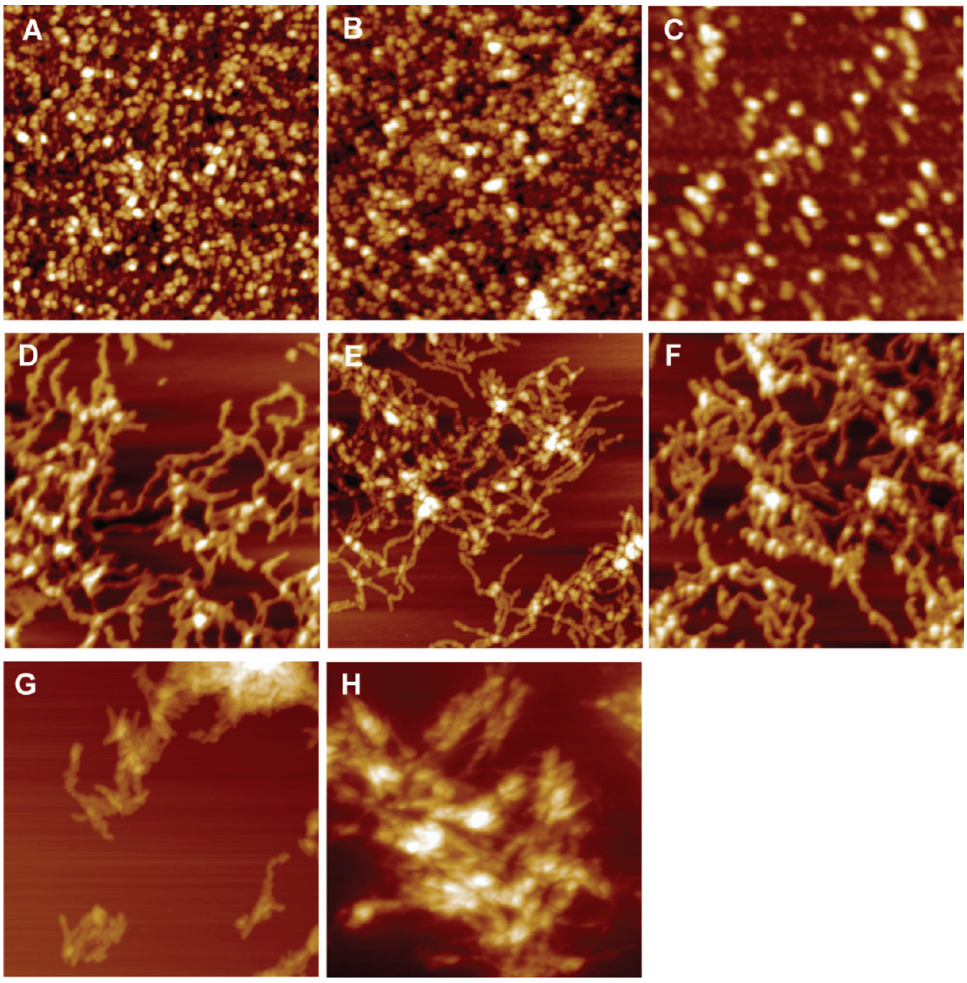

Figure 2. AFM height images of the self-assembled nanostructures of A_9K (1.0 mM) in the presence of (A) 1.0 mM $NaClO_3$, (B) 1.0 mM $NaNO_3$, (C) 1.0 mM NaBr, (D) 1.0 mM NaCl, (E) 0.5 mM Na_2SO_4, (F) 0.5 mM Na_2HPO_4, (G) 0.33 mM Na_3PO_4, and (H) 0.33 mM $Na_3C_6H_5O_7$. The scanning size is 1.0 × 1.0 μm^2, and the height scale is 30 nm for all of the images.

their merging and elongation.[8,41] Interestingly, in the cases of Cl^-, SO_4^{2-}, HPO_4^{2-}, PO_4^{3-}, and $C_6H_5O_7^{3-}$, the primary aggregates could fuse and grow into long fibrils, but in the cases of ClO_3^-, NO_3^-, and Br^-, no such behavior was observed. It is well-known that the directional growth of peptide nanostructures along their long axis is usually associated with hydrogen bonding. Hence, the above results indicate that Cl^-, SO_4^{2-}, HPO_4^{2-}, PO_4^{3-}, and $C_6H_5O_7^{3-}$ could facilitate the axial hydrogen bonding, while ClO_3^-, NO_3^-, and Br^- inhibit it. Note, however, that the resultant fibrils in the former case are not strictly linear in shape. In fact, random bending along the long fibrillar axis seems to be dominant. We attributed this feature to the random packing between the primary aggregates as a result of salt addition.

To help assess the effect of different salts on the aggregation potential of A_9K, the turbidity assay was also performed by monitoring the absorbance at 350 nm. As shown in Figure 3, relatively lower turbidity values were obtained from solutions containing $NaClO_3$, $NaNO_3$, NaBr, and the control experiment, whereas the turbidity increased significantly from solutions containing NaCl, Na_2SO_4, Na_2HPO_4, Na_3PO_4, and $Na_3C_6H_5O_7$. The increased turbidity values are consistent with the increased sizes and extent of aggregation as revealed from the AFM results, especially in the cases of Na_3PO_4 and $Na_3C_6H_5O_7$ where large fibril bundles were formed. The differences suggest that the latter systems favored A_9K aggregation associated with length growth of nanofibrils. Thus turbidity results are broadly consistent with the AFM observations. Here, if the absorbance values were taken as the criterion to assess the relative efficiency of different anions, the order of promotion of the aggregation of A_9K should be $ClO_3^- < NO_3^- \leq Br^- < Cl^- < SO_4^{2-} < HPO_4^{2-} < PO_4^{3-} < C_6H_5O_7^{3-}$.

To assess the effects of different salts on peptide conformation within the assembled nanostructures, CD measurements were performed under the same conditions as used for the control. The CD spectra as shown in Figure 4 are similar to those of A_9K without any added salts (Figure 1C), with a positive peak at 196−200 nm and a negative peak at 218−221.5 nm, revealing the predominance of β-sheet conformation in all cases in spite of the great morphological variations. However, slight shifts of the positive/negative peaks occurred in the presence of salts. While the CD signals under 200 nm are prone to the influence of solution conditions (e.g., strong absorption from ions) and thus are less informative, the measurements above 200 nm are more reliable. Shifts in the negative peak around 218 nm are usually associated with distortion of β-sheets.[46,47] Taking the CD spectrum of A_9K itself (Figure 1C, negative minimum at 219 nm)

Table 1. Heights and Lengths of the Nanostructures Formed in the Solutions of A_9K Containing Sodium Salts with Different Anions

	nanostructure	height[a] (nm)	length[a] (nm)
A_9K	spheres	3.2 ± 0.6	
	rods	3.0 ± 0.5	<100
$A_9K/NaClO_3$	spheres	3.7 ± 0.5	
$A_9K/NaNO_3$	spheres	4.0 ± 0.6	
$A_9K/NaBr$	spheres	3.8 ± 0.8	
$A_9K/NaCl$	spheres	4.3 ± 0.7	
	entangled fibrils	3.8 ± 0.5	>500
A_9K/Na_2SO_4	spheres	4.5 ± 0.8	
	entangled fibrils	4.0 ± 0.5	>500
A_9K/Na_2HPO_4	spheres	5.0 ± 0.5	
	entangled fibrils	4.0 ± 1.0	>500
A_9K/Na_3PO_4	spheres		
	closely packed fibrils	5.5 ± 0.7	>500
$A_9K/Na_3C_6H_5O_7$	spheres		
	closely packed fibril bundles		>500

[a] Heights rather than widths were obtained to evaluate the diameters of different nanoaggregates due to the effect of AFM tip-related convolution.[45] For the same reason, the lengths of the nanosphere stacks were exaggerated and are therefore not given. In the cases of A_9K/Na_3PO_4 and $A_9K/Na_3C_6H_5O_7$, it is hard to measure the heights of spheres and/or fibrils due to their close packing.

as reference, the negative peak shifts in different cases are listed in Table 2. ClO_3^- caused the largest downward shift (−1.0 nm) of the peak, while PO_4^{3-} and $C_6H_5O_7^{3-}$ caused the largest upward shifts (2.5 and 1.5 nm, respectively). In contrast, all of the other anions caused moderate peak shifts. Such an order is roughly consistent with the efficiency of different ions in promoting A_9K aggregation, indicating that one important means of the anions to affect peptide aggregation is to tune the internal molecular arrangement. However, it should also be noted that although the A_9K nanostructures obtained under different salts could be roughly classified into two categories, the spherical nanostacks and the long nanofibrils, it is perhaps difficult to associate the small CD peak shifts with these morphological variations. These observations hence imply that other mechanisms of the ion effects may also exist and work together to tune peptide aggregation. Moreover, the amplitude or intensity of the CD signal also exhibited variations in peak intensity. Addition of ions in all cases led to the reduction of the amplitude, with the largest reduction from PO_4^{3-} and $C_6H_5O_7^{3-}$ and the smallest reduction from ClO_3^-. Because changes in intensity are indicative of the relative amount of peptide molecules arranged into the ordered β-sheet structure,[48] the observations from Figure 4 simply suggest shifts in the population of secondary structures upon addition of different ions associated with different morphological changes. It should, however, be noted that in the present systems the aggregation-induced scattering of the circularly polarized light can also contribute to the signal and cause irregularity.

Effect of Cations on the Self-Assembly of A_9K. To assess the effects of cations on the self-assembly of A_9K molecules, we further imaged the morphologies of A_9K nanoaggregates formed in the presence of zinc salts. The two representative AFM images obtained from $Zn(NO_3)_2$ and $ZnSO_4$ are shown in Figure 5, with key parameters given in Table 3. As it can be seen, in the case of

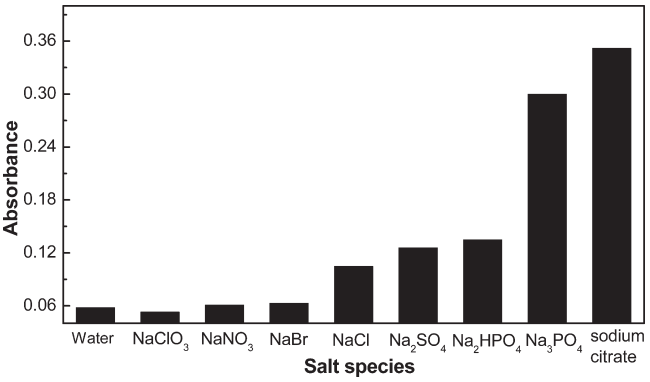

Figure 3. Turbidity results measured from A_9K solutions (1.0 mM) in the presence of different sodium salts (1.0 mM for $NaClO_3$, $NaNO_3$, NaBr, NaCl, and NaAc, 0.5 mM for Na_2SO_4 and Na_2HPO_4, 0.33 mM for Na_3PO_4 and $Na_3C_6H_5O_7$). Turbidity results were presented as the absorbance values at 350 nm.

$Zn(NO_3)_2$ (Figure 5A), only spherical nanostacks are present, similar to the case of $NaNO_3$ (Figure 2B). In the case of $ZnSO_4$ (Figure 5B), there are many long fibrillar structures, similar to the case of Na_2SO_4 (Figure 2E). These results show that the effects of salts on the self-assembled structures of A_9K mainly come from the anions, as expected.

Effects of Anions on the Self-Assembly of Other Cationic Amphiphilic Peptides. To test whether the above anion effects are applicable for tuning the self-assembly of other amphiphilic peptides, we further designed and synthesized another peptide molecule I_3K. As shown in Figure 6A, I_3K has a hydrophobic chain consisting of three isoleucine residues. Lysine bearing a cationic charge over the normal pH range works as the hydrophilic head. I_3K formed semiflexible nanotubes with smooth outer surface in aqueous solution, as shown in Figures 6B. Their contour lengths were typically on the order of micrometers. In contrast, their heights were constant at 10.0 ± 1.0 nm. However, after adding sodium salts with different counterions into the solution, the self-assembled nanostructures of I_3K were considerably altered and the features are evident from the different cases shown in Figure 7. In the group of $NaClO_3$, $NaNO_3$, and NaBr (Figure 7A−C, respectively), the original long tubular structures of I_3K broke down to many globular nanostacks and short nanorods with lengths ranging from nanometers to submicrometers. In the group of NaCl, Na_2SO_4, Na_2HPO_4, Na_3PO_4, and $Na_3C_6H_5O_7$ (Figure 7D−H, respectively), however, the self-assembled nanostructures showed new features in morphology, typically reflected in greater diameter and much rougher outer surface. Furthermore, the nanotubes are prone to becoming entangled and bundled with each other, especially in the cases of Na_3PO_4 and $Na_3C_6H_5O_7$ where a gel-like state was induced to form due to high degree of fibril association with each other. These results indicate that ClO_3^-, Br^-, and NO_3^- tend to break down the I_3K tubular structures to smaller lengths, while Cl^-, SO_4^{2-}, HPO_4^{2-}, PO_4^{3-}, and $C_6H_5O_7^{3-}$ promote the increase in diameter and the lateral packing of the nanotubes.

I_3K nanotubes formed in pure aqueous solution (pH 7, with the lowest ionic strength) were found to be very stable against heating, pH adjustment, diluting, and polar organic solvents.[9] This range of stability was however found to be different when salt was added. In almost all cases studied here, salt addition substantially reduced the stability or robustness of the nanostructures.

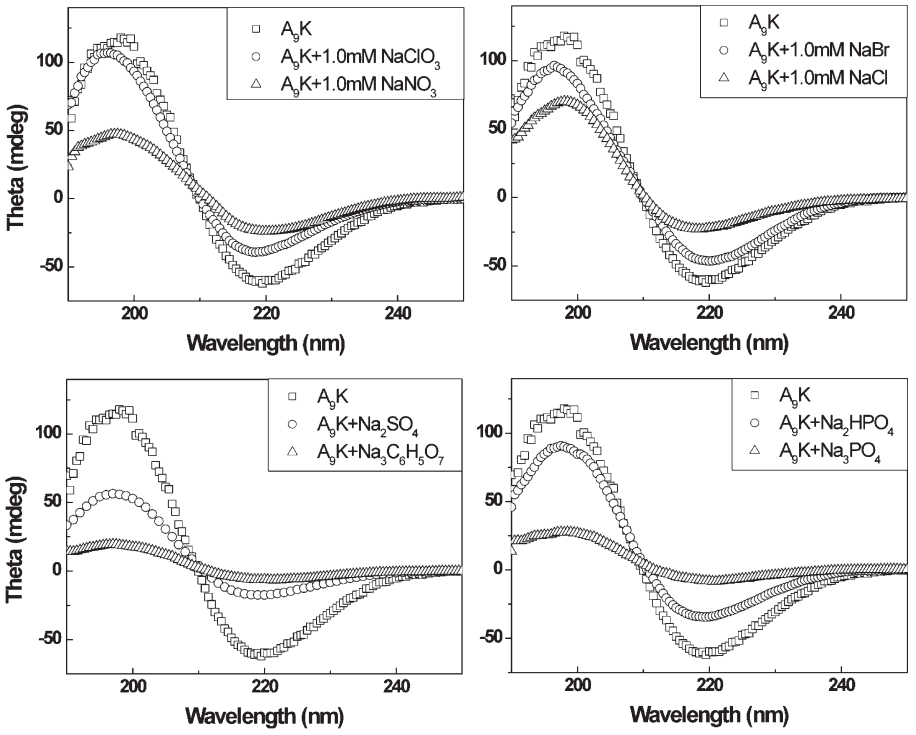

Figure 4. CD spectra measured from A_9K solutions (1.0 mM, pH 7.0) in the presence of different sodium salts.

Table 2. Shifts in the Negative CD Peak from A_9K Solutions with Different Sodium Salts with Reference to the A_9K Peak without Any Added Salt

	$NaClO_3$	$NaNO_3$	NaBr	NaCl	Na_2SO_4	Na_2HPO_4	Na_3PO_4	$Na_3C_6H_5O_7$
peak shift (nm)	−1.0	0.5	0.5	−0.5	0.5	0	2.5	1.5

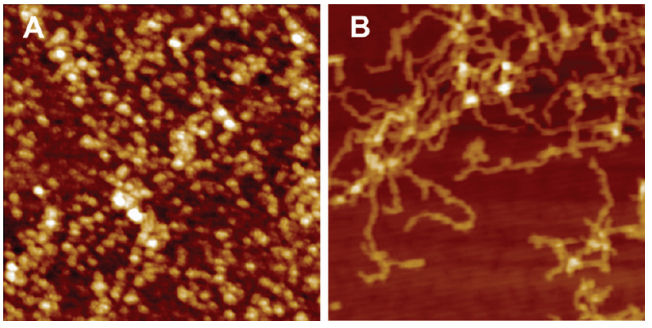

Figure 5. AFM height images of the A_9K nanostructures produced in the solutions of 1.0 mM A_9K (pH 7.0) with (A) 0.5 mM $Zn(NO_3)_2$ and (B) 0.5 mM $ZnSO_4$. The image size is 1.0 × 1.0 μm^2, and the height scale is 30 nm for all of the images taken.

Table 3. Heights and Lengths of the Structures Formed in the Solutions of A_9K in the Presence of 0.5 mM Zinc Salts with Different Anions

	structure	height (nm)	length (nm)
$A_9K/Zn(NO_3)_2$	spheres	3.8 ± 1.0	
$A_9K/ZnSO_4$	spheres	4.3 ± 1.2	
	entangled fibrils	4.0 ± 0.5	>1000

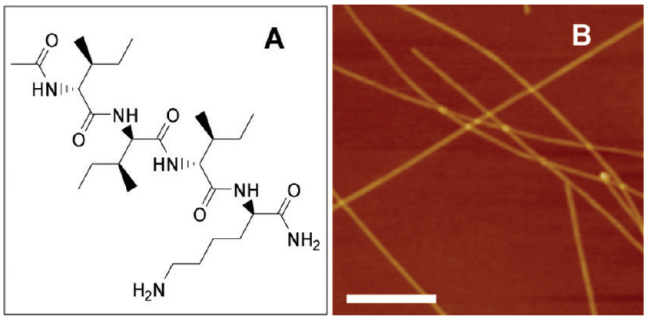

Figure 6. (A) Molecular structure of I_3K and (B) AFM height image (scale bar = 500 nm, height scale = 50 nm) of the self-assembled nanostructures of I_3K at 2.0 mM and pH 7.0.

While the exact underlying mechanism remains unclear, we suspect that salts may affect peptide self-assembly through a complicated combination of ion binding and electrostatic screening. Such combined action of salts can further affect hydrophobic interaction and dispersion forces through adjusting molecular hydration, as will be discussed in the following.

The turbidity values of the I_3K solutions in the presence of different salts were also obtained to evaluate anion efficiency in promoting the aggregation of I_3K. As seen from Figure 8, the order was $ClO_3^- < NO_3^- \approx Br^- < Cl^- < SO_4^{2-} < HPO_4^{2-}$, also

dx.doi.org/10.1021/jp205987w |J. Phys. Chem. B 2011, 115, 11862–11871

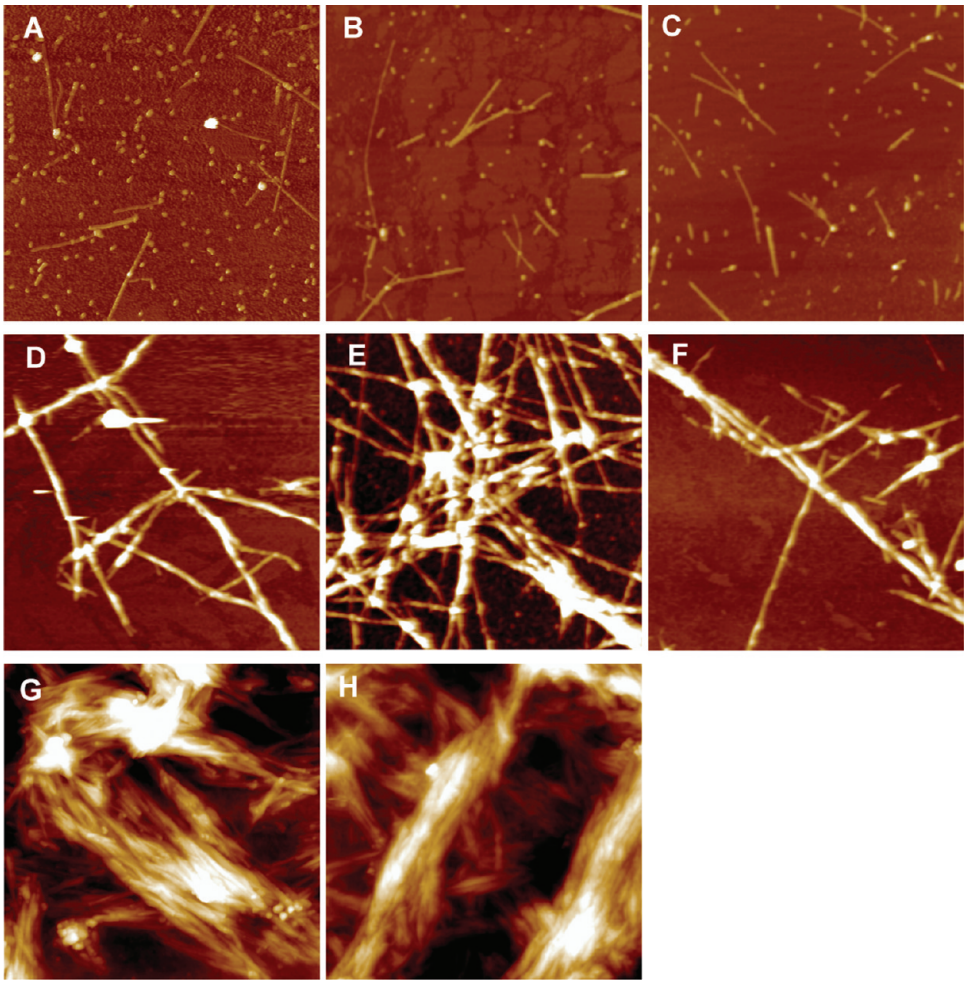

Figure 7. AFM height images of the self-assembled nanostructures of I_3K (2.0 mM, pH 7.0) in the presence of (A) 1.0 mM $NaClO_3$, (B) 1.0 mM $NaNO_3$, (C) 1.0 mM NaBr, (D) 1.0 mM NaCl, (E) 0.5 mM Na_2SO_4, (F) 0.5 mM Na_2HPO_4, (G) 0.33 mM Na_3PO_4, and (H) 0.33 mM $Na_3C_6H_5O_7$. The size is 2.0 × 2.0 μm^2 for all of the images, while the height scale is 30 nm for images A−F and 60 nm for images G and H.

in good agreement with the results of A_9K. The turbidity results for $C_6H_5O_7^{3-}$ and PO_4^{3-} salts are not shown here, but they clearly follow the above order because they induced the strongest aggregation.

More experiments to test the efficiency of the anions in promoting the aggregation of other two cationic amphiphilic peptides, A_6K and I_4K, have also been performed. The results (data not shown) all revealed similar anion series to those obtained from A_9K and I_3K. Such anion effects must thus be common in tuning the self-assembly of cationic amphiphilic peptides.

DISCUSSION

In aqueous solutions with little or no added salt, peptides such as A_9K and I_3K self-assemble into nanorods (lengths around 100 nm and diameters around 3 nm) and long nanofibers (diameters around 10 nm and lengths over 1 μm), respectively. Anion effects on peptide nanostructuring can be divided into two types. While ClO_3^-, NO_3^-, and Br^- favor smaller peptide nanoaggregates (nanostacks and shorter nanorods) and prohibit their further growth, Cl^-, SO_4^{2-}, HPO_4^{2-}, PO_4^{3-}, and $C_6H_5O_7^{3-}$ enhance the growth into peptide nanorods and nanofibers that are even bigger than those formed without salts. The order of efficiency of different anions in promoting peptide aggregation is the same for all of the cationic peptides studied: $ClO_3^- < NO_3^- \approx Br^- < Cl^- < SO_4^{2-} < HPO_4^{2-} < PO_4^{3-} < C_6H_5O_7^{3-}$. Divalent and trivalent anions have larger efficiency than monovalent anions in promoting the aggregation of peptide nanostructures.

Figure 9 lists the Hofmeister series of the anions studied in this work,[36,40,49,50] and the order is the same as the sequence of increased surface charge density; that is, the anions on the left side have low surface charge densities and are weakly hydrated in solution. These anions tend to coordinate with weakly positively charged residues on proteins in solution according to the Law of Matching Water Affinities.[49,51,52] In contrast, the anions on the right side of Figure 9 have high surface charge densities and are strongly hydrated in solution, thus staying away from weakly positively charged residues on proteins. Binding of anions to proteins through ion pairing can increase or decrease solubility depending on the outcome of net charges, even though this process often leads to structural unfolding (chaotropic effect). Conversely, competition for water hydration can lead to the decline of protein solubility (kosmotropic effect). In the present case, the efficiency order of different anions in promoting peptide aggregation follows approximately the Hofmeister anion series.

Hofmeister effects have also been utilized to describe interesting electrostatic screening effects observed in the micellization

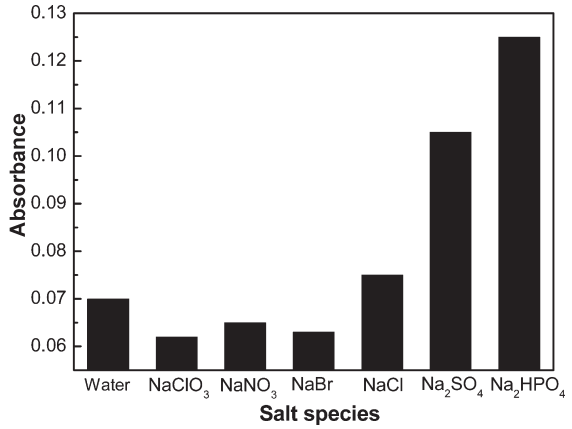

Figure 8. Turbidity results of I_3K solutions (2.0 mM, pH 7.0) in the absence and presence of different sodium salts, with the exact conditions kept the same as in AFM imaging. Turbidity values of the I_3K solutions in the presence of $Na_3C_6H_5O_7$ and Na_3PO_4 were absent because gel-like structures were formed in these two cases, which made turbidity measurements meaningless.

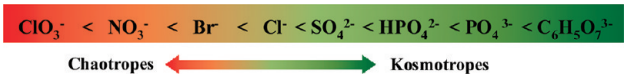

Figure 9. Efficiency order of anions in promoting aggregation of amphiphilic peptides follows approximately Hofmeister anion sequence.[33,36,40,49,50,52−54]

of traditional surfactants.[55,56] In the present system, charge screening certainly functions to affect the peptide aggregation; however, we cannot explain all of the experimental findings using charge screening theory only, which is reasoned as follows. Collins et al. have proposed the concept of matching water affinities to rationalize different interactions between oppositely charged ions.[49,52,57] They demonstrated that oppositely charged ions with equal water affinity tend to form contact ion pairs in solutions, whereas those with differing water affinities tend to stay apart.[52] In the present case, the positively charged amine groups (side chain of lysine) are weakly hydrated and have a low water affinity.[52,57] Hence, the weakly hydrated anions of ClO_3^-, NO_3^-, and Br^- more readily form contact ion pairs with the lysine ammonium group, allowing the peptides to form compact hydrogen-bonded structures with the "neutralized" lysine ammonium residues close together, while strongly hydrated anions of Cl^-, SO_4^{2-}, HPO_4^{2-}, PO_4^{3-}, and $C_6H_5O_7^{3-}$ tend to stay away from the weakly hydrated positively charged lysine residues, causing the peptides to form extended hydrogen-bonded structures that keep the "un-neutralized" lysine residues far apart. That is to say, chaotropes are more effective than kosmotropes in screening the positive charges on peptides and reducing charge repulsion. Then if only charge screening effect works, ClO_3^-, NO_3^-, and Br^- should be more effective than Cl^-, SO_4^{2-}, HPO_4^{2-}, PO_4^{3-}, and $C_6H_5O_7^{3-}$ in promoting peptide aggregation in consideration of higher charge screening results in less charge repulsion and thus higher aggregation propensity, which will result in a reversed Hofmeister series as for traditional surfactants.[58−60] However, this obviously contradicts our present experimental findings.

Recent time-resolved and thermodynamic investigations of water molecules in salt solutions have revealed that ions have little effect on the bulk water structure.[24,51,61] Instead, direct interfacial interactions between ions and macromolecules play crucial roles in imparting macromolecular solubility and stability through Hofmeister effects of salts.[24,34,43] Von Hoppel and his co-workers[62] analyzed ion effects using a polyacrylamide column as a model for the peptide backbone and demonstrated direct ion interactions with the amide groups. Cremer et al.[24,43,52−63] have proposed that the anions could interact directly with the macromolecules through three modes. First, kosmotropic anions can polarize water molecules that are hydrogen-bonded to the amide moieties. Second, chaotropic anions can directly bind to the amide groups. Third, both kosmotropic and chaotropic anions can interfere with hydration of the hydrophobic segments of the molecules by raising surface tension. The first and third modes of action lead to salting-out, but the second one leads to salting-in, and the combined modes of action together determine the specific effect for a particular ion.

Figure 10 provides a schematic representation of the observed ion effects on promoting peptide aggregation via the direct interactions between the anions and the peptides. The anions play different roles by delicately adjusting their balance of different modes of action. The anions can associate to a varying extent with the positively charged amine head groups. Both charge screening and disruption of hydration of the hydrophobic segments favor peptide aggregation.[33,49] The anions can also interact with peptide backbones following Hofmeister series. Chaotropic anions tend to bind directly to the amide groups, increasing the solubility of peptides (Figure 10A) and favoring disaggregation. In contrast, kosmotropic anions compete for water molecules in the peptide hydration layer (Figure 10B), make them unavailable to solvate the amide groups, decreasing peptide solubility and favoring peptide aggregation. For kosmotropic anions such as SO_4^{2-}, HPO_4^{2-}, PO_4^{3-}, and $C_6H_5O_7^{3-}$, all of the factors considered above favor peptide aggregation. For chaotropic anions, the situation is more complex because the opposite effects exist; that is, charge screening and increase in hydration cost favor peptide aggregation while direct binding of the anions to peptides disfavors aggregation. The outcome is that anions such as ClO_3^- disfavor aggregation, while those like Cl^- intensify aggregation. Divalent and trivalent anions are clearly more effective in promoting peptide aggregation than monovalent anions. Apart from the kosmotropic effect described above, divalent anions can also bridge with two charged amino acid charges,[24,55] thus strengthening aggregation propensity.

The effect of polarizability of the ions in the context of protein solubility and stabilization remains poorly understood. For the highly polarizable anions such as ClO_3^- and NO_3^-, they tend to be strongly attracted to the peptide molecules because they experience large attractive ionic dispersion potentials, while for less polarizable anions such as SO_4^{2-} and HPO_4^{2-}, electrostatic forces and interference with the first hydration layer may dominate. In consideration of Cl^- and Br^-, both of which are halogen, the significant difference in their aggregation promoting and inhibiting ability is linked to their location in the Hofmeister anion sequence, consistent with Cl^- being more kosmotropic and Br^- being more chaotropic. This explanation is also supported by the observed preference of Br^- to the interface.[54]

The effects of anions on the direction of aggregation of all our peptides are consistent with the Hofmeister series. This correlation is not firmly reflected from the CD spectra. As demonstrated by Ninham et al., Hofmeister effects arise from a complex interplay of both electrostatic and non-electrostatic forces, often

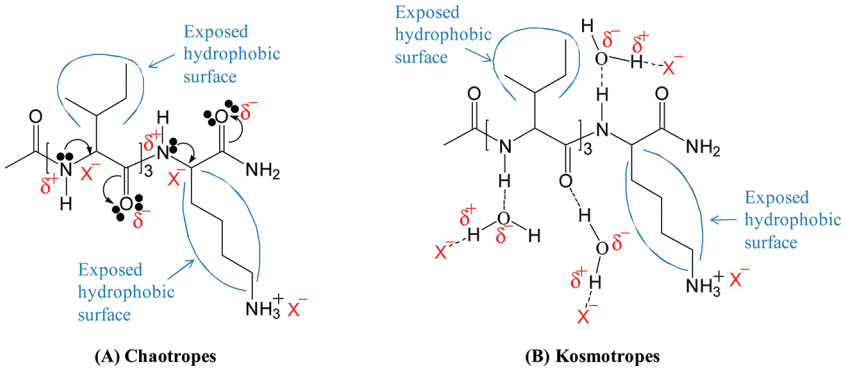

Figure 10. Schematic illustration of different mechanisms of interaction between chaotropic and kosmotropic anions and peptides.

resulting in complications in observations and making interpretation ambiguous.[40,54] Apart from electrostatic interactions, the present systems involve hydration, hydrogen bonding, hydrophobicity, and so on. Hydrogen bonding represents specific signatures in CD signal and is only one aspect among the various elements affecting peptide self-assembly, while structural reorganization can arise from any of the above interactions or a combination of them.

CONCLUSIONS

This study has examined the influence of different ions on the self-assembled nanostructures of cationic amphiphilic peptides. The results show that anions exhibit more pronounced effects than cations on the nanostructure. While ClO_3^-, NO_3^-, and Br^- inhibited the growth of nanostacks and very short nanorods into longer nanorods as observed in A_9K solution, Cl^-, SO_4^{2-}, HPO_4^{2-}, PO_4^{3-}, and $C_6H_5O_7^{3-}$ favored the growth of A_9K structures to form longer and bigger intersecting nanofibers. Similar results were observed for I_3K and two other cationic peptides, indicating that such anion effects must be rather common. The order of efficiency of the anions in promoting peptide aggregation followed the Hofmeister sequence. Such specific ion effects may be attributed to a complex interplay of both electrostatic and non-electrostatic forces. Although the exact mechanisms behind different self-assembly processes remain unclear, the rationalization by considering electrostatic screening, ion binding, and its implication to hydrophobic interaction offers a consistent description of the relatively different ion effects as observed. The present study provides a clear perspective of using ions as effective and simple handles to control peptide nanostructures in addition to the rational design of molecular structure. Further studies are underway to establish whether similar rules are held for anionic peptide amphiphiles.

ASSOCIATED CONTENT

Supporting Information. The pH values of I_3K solution in the presence of different salts. This material is available free of charge via the Internet at http://pubs.acs.org.

AUTHOR INFORMATION

Corresponding Author

*Phone: 86-532-86981569 (H.X.), 44-161-3063926 (J.R.L.). E-mail: xuh@upc.edu.cn (H.X.), j.lu@manchester.ac.uk (J.R.L.).

ACKNOWLEDGMENT

This work was supported by the National Natural Science Foundation of China (Grant Numbers 20773164, 21003160), the Natural Science Foundation of Shandong Province of China (ZR2009BQ003), the Fundamental Research Funds for the Central Universities (09CX04036A), the Royal Society (London) under a Sino-British Fellowship Trust grant and the UK Physical Sciences and Engineering Research Council (EPSRC).

REFERENCES

(1) Whitesides, G.; Mathias, J.; Seto, C. *Science* **1991**, *254*, 1312–1319.
(2) Nowak, A. P.; Breedveld, V.; Pakstis, L.; Ozbas, B.; Pine, D. J.; Pochan, D.; Deming, T. J. *Nature* **2002**, *417*, 424–428.
(3) Holmes, T. C.; de Lacalle, S.; Su, X.; Liu, G.; Rich, A.; Zhang, S. *Proc. Natl. Acad. Sci. U.S.A.* **2000**, *97*, 6728–6733.
(4) Hartgerink, J. D.; Beniash, E.; Stupp, S. I. *Proc. Natl. Acad. Sci. U.S.A.* **2002**, *99*, 5133–5138.
(5) Vauthey, S.; Santoso, S.; Gong, H.; Watson, N.; Zhang, S. *Proc. Natl. Acad. Sci. U.S.A.* **2002**, *99*, 5355–5360.
(6) Santoso, S.; Hwang, W.; Hartman, H.; Zhang, S. *Nano Lett.* **2002**, *2*, 687–691.
(7) von Maltzahn, G.; Vauthey, S.; Santoso, S.; Zhang, S. *Langmuir* **2003**, *19*, 4332–4337.
(8) Xu, H.; Wang, J.; Han, S.; Wang, J.; Yu, D.; Zhang, H.; Xia, D.; Zhao, X.; Waigh, T. A.; Lu, J. R. *Langmuir* **2008**, *25*, 4115–4123.
(9) Xu, H.; Wang, Y.; Ge, X.; Han, S.; Wang, S.; Zhou, P.; Shan, H.; Zhao, X.; Lu, J. R. *Chem. Mater.* **2010**, *22*, 5165–5173.
(10) Zhao, X.; Pan, F.; Xu, H.; Yaseen, M.; Shan, H.; Hauser, C. A. E.; Zhang, S.; Lu, J. R. *Chem. Soc. Rev.* **2010**, *39*, 3480–3498.
(11) Reches, M.; Gazit, E. *Science* **2003**, *300*, 625–627.
(12) Firth, A.; Aggeli, A.; Burke, J. L.; Yang, X.; Kirkham, J. *Nanomedicine* **2006**, *1*, 189–199.
(13) Wang, S.; Ge, X.; Xue, J.; Fan, H.; Mu, L.; Li, Y.; Xu, H.; Lu, J. R. *Chem. Mater.* **2011**, *23*, 2466–2474.
(14) Zhang, S.; Yan, L.; Altman, M.; Lassle, M.; Nugent, H.; Frankel, F.; Lauffenburger, D. A.; Whitesides, G. M.; Rich, A. *Biomaterials* **1999**, *20*, 1213–1220.
(15) Whitehouse, C.; Fang, J.; Aggeli, A.; Bell, M.; Brydson, R.; Fishwick, C. W.; Henderson, J. R.; Knobler, C. M.; Owens, R. W.; Thomson, N. H.; Smith, D. A.; Boden, N. *Angew. Chem., Int. Ed.* **2005**, *44*, 1965–1968.
(16) Wang, X.; Corin, K.; Baaske, P.; Wienken, C. J.; Jerabek-Willemsen, M.; Duhr, S.; Braun, D.; Zhang, S. *Proc. Natl. Acad. Sci. U.S.A.* **2011**, *108*, 9049–9054.
(17) Ge, B.; Yang, F.; Yu, D.; Liu, S.; Xu, H. *PLoS ONE* **2010**, *5*, e10233.
(18) Chen, C.; Pan, F.; Zhang, S.; Hu, J.; Cao, M.; Wang, J.; Xu, H.; Zhao, X.; Lu, J. R. *Biomacromolecules* **2010**, *11*, 402–411.

(19) Zhang, S.; Marini, D. M.; Hwang, W.; Santoso, S. *Curr. Opin. Chem. Biol.* **2002**, *6*, 865–871.
(20) Carrick, L. M.; Aggeli, A.; Boden, N.; Fisher, J.; Ingham, E.; Waigh, T. A. *Tetrahedron* **2007**, *63*, 7457–7467.
(21) Song, Y.; Challa, S. R.; Medforth, C. J.; Qiu, Y.; Watt, R. K.; Pena, D.; Miller, J. E.; van Swol, F.; Shelnutt, J. A. *Chem. Commun.* **2004**, *9*, 1044–1045.
(22) Yan, X.; He, Q.; Wang, K.; Duan, L.; Cui, Y.; Li, J. *Angew. Chem.* **2007**, *119*, 2483–2486.
(23) Yan, X.; Cui, Y.; He, Q.; Wang, K.; Li, J.; Mu, W.; Wang, B.; Ou-Yang, Z. C. *Chem.—Eur. J.* **2008**, *14*, 5974–5980.
(24) Yang, H.; Pritzker, M.; Fung, S. Y.; Sheng, Y.; Wang, W.; Chen, P. *Langmuir* **2006**, *22*, 8553–8562.
(25) Mart, R. J.; Osborne, R. D.; Stevens, M. M.; Ulijn, R. V. *Soft Matter* **2006**, *2*, 822–835.
(26) Fairman, R.; Åkerfeldt, K. S. *Curr. Opin. Struct. Biol.* **2005**, *15*, 453–463.
(27) Hofmeister, F. *Arch. Exp. Pathol. Pharmacol.* **1888**, *24*, 247–260.
(28) Hamaguchi, K.; Geiduschek, E. P. *J. Am. Chem. Soc.* **1962**, *84*, 1329–1338.
(29) Collins, K. D.; Washabaugh, M. W. *Q. Rev. Biophys.* **1985**, *18*, 323–422.
(30) Zhang, Y.; Cremer, P. S. *Curr. Opin. Chem. Biol.* **2006**, *10*, 658–663.
(31) Omta, A. W.; Kropman, M. F.; Woutersen, S.; Bakker, H. J. *Science* **2003**, *301*, 347–349.
(32) Batchelor, J. D.; Olteanu, A.; Tripathy, A.; Pielak, G. J. *J. Am. Chem. Soc.* **2004**, *126*, 1958–1961.
(33) Zhang, Y.; Furyk, S.; Bergbreiter, D. E.; Cremer, P. S. *J. Am. Chem. Soc.* **2005**, *127*, 14505–1410.
(34) Leontidis, E. *Curr. Opin. Colloid Interface Sci.* **2002**, *7*, 81–91.
(35) Kunz, W.; Henle, J.; Ninham, B. W. *Curr. Opin. Colloid Interface Sci.* **2004**, *9*, 19–37.
(36) Pinna, M. C.; Salis, A.; Monduzzi, M.; Ninham, B. W. *J. Phys. Chem. B* **2005**, *109*, 5406–5408.
(37) Bauduin, P.; Nohmie, F.; Touraud, D.; Neueder, R.; Kunz, W.; Ninham, B. W. *J. Mol. Liq.* **2006**, *123*, 14–19.
(38) Lund, M.; Jungwirth, P.; Woodward, C. E. *Phys. Rev. Lett.* **2008**, *100*, 258105.
(39) Bosttöm, M.; Tavares, F. W.; Finet, S.; Skouri-Panet, F.; Tardieu, A.; Ninham, B. W. *Biophys. Chem.* **2005**, *117*, 217–224.
(40) Kunz, W.; Lo Nostro, P.; Ninham, B. W. *Curr. Opin. Colloid Interface Sci.* **2004**, *9*, 1–18.
(41) Wang, J.; Han, S.; Meng, G.; Xu, H.; Xia, D.; Zhao, X.; Schweins, R.; Lu, J. R. *Soft Matter* **2009**, *5*, 3870–3878.
(42) Bucak, S.; Cenker, C.; Nasir, I.; Olsson, U.; Zackrisson, M. *Langmuir* **2009**, *25*, 4262–4265.
(43) Yang, J. T.; Wu, C. S. C.; Martinez, H. M. *Methods Enzymol.* **1986**, *130*, 208–269.
(44) Rochet, J.-C.; Lansbury, P. T. *Curr. Opin. Struct. Biol.* **2000**, *10*, 60–68.
(45) Anderson, M.; Bocharova, O. V.; Makarava, N.; Breydo, L.; Salnikov, V. V.; Baskakov, I. V. *J. Mol. Biol.* **2006**, *358*, 580–596.
(46) Paramonov, S. E.; Jun, H. W.; Hartgerink, J. D. *J. Am. Chem. Soc.* **2006**, *128*, 7291–7298.
(47) Manning, M. C.; Illangasekare, M.; W. Woody, R. *Biophys. Chem.* **1988**, *31*, 77–86.
(48) Schneider, J. P.; Pochan, D. J.; Ozbas, B.; Rajagopal, K.; Pakstis, L.; Kretsinger, J. *J. Am. Chem. Soc.* **2002**, *124*, 15030–15037.
(49) Collins, K. D. *Methods* **2004**, *34*, 300–311.
(50) Ebel, C.; Faou, P.; Kernel, B.; Zaccai, G. *Biochemistry* **1999**, *38*, 9039–9047.
(51) Collins, K. D. *Biophys. Chem.* **2006**, *119*, 271–281.
(52) Collins, K. D.; Neilson, G. W.; Enderby, J. E. *Biophys. Chem.* **2007**, *128*, 95–104.
(53) Giner, I.; Pera, G.; Lafuente, C.; Lopez, M. C.; Cea, P. *J. Colloid Interface Sci.* **2007**, *315*, 588–596.
(54) Salis, A.; Monduzzi, M.; Ninham, B. W. Hofmeister Effects in Enzymatic Activity, Colloid Stability and pH Measurements: Ion-Dependent Specificity of Intermolecular Forces. In *Nanoparticles and Nanodevices in Biological Applications*; Bellucci, S., Ed.; Springer-Verlag: Berlin, Heidelberg, 2009; pp 159−194.
(55) Jiang, N.; Li, P.; Wang, Y.; Wang, J.; Yan, H.; Thomas, R. K. *J. Colloid Interface Sci.* **2005**, *286*, 755–760.
(56) Lin, H. P.; Kao, C. P.; Mou, C. Y.; Liu, S. B. *J. Phys. Chem. B* **2000**, *104*, 7885–7894.
(57) Collins, K. D. *Biophys. J.* **1997**, *72*, 65–76.
(58) Maiti, K.; Mitra, D.; Guha, S.; Moulik, S. P. *J. Mol. Liq.* **2009**, *146*, 44–51.
(59) Naskar, B.; Dan, A.; Ghosh, S.; Moulik, S. P. *Carbohydr. Polym.* **2010**, *81*, 700–706.
(60) Heyda, J.; Lund, M.; Oncák, M.; Slavícek, P.; Jungwirth, P. *J. Phys. Chem. B* **2010**, *114*, 10843–10852.
(61) Omta, A. W.; Kropman, M. F.; Woutersen, S.; Bakker, H. J. *J. Chem. Phys.* **2003**, *119*, 12457–12461.
(62) Von Hippel, P. H.; Peticolas, V.; Schack, L.; Karlson, L. *Biochemistry* **1973**, *12*, 1256–1264.
(63) Zhang, Y. J.; Furyk, S.; Sagle, L. B.; Cho, Y.; Bergbreiter, D. E.; Cremer, P. S. *J. Phys. Chem. C* **2007**, *111*, 8916–8924.